Journal of ELECTRONIC MATERIALS, Vol. 40, No. 10, 2011
DOI: 10.1007/s11664-011-1721-y
© 2011 TMS

Preparation and Characterization of Ultralow-Dielectric-Constant Porous SiCOH Thin Films Using 1,2-Bis(triethoxysilyl)ethane, Triethoxymethylsilane, and a Copolymer Template

SHUANG FU,[1,2] KE-JIA QIAN,[1] SHI-JIN DING,[1,3] and DAVID WEI ZHANG[1]

1.—State Key Laboratory of ASIC and System, Department of Microelectronics, Fudan University, Shanghai 200433, China. 2.—Department of Material Science, Fudan University, Shanghai 200433, China. 3.—e-mail: sjding@fudan.edu.cn

Ultralow-dielectric-constant (k) porous SiCOH films have been prepared using 1,2-bis(triethoxysilyl)ethane, triethoxymethylsilane, and a poly(ethylene oxide)–poly(propylene oxide)–poly(ethylene oxide) triblock copolymer template by means of spin-coating. The resulting films were characterized by cross-section scanning electron microscopy, small-angle x-ray diffraction, atomic force microscopy, Fourier-transform infrared spectroscopy, nanomechanical testing, and electrical measurements. Thermal treatment at 350°C for 2 h resulted in the formation of ultralow-k films with k of ~2.0, leakage current density of 3×10^{-8} A/cm^2 at 1 MV/cm, reduced modulus (E_r) of ~4.05 GPa, and hardness (H) of ~0.32 GPa. After annealing between 400°C and 500°C for 30 min, the resulting films showed fluctuant k values of 1.85 to 2.22 and leakage current densities of 3.7×10^{-7} A/cm^2 to 3×10^{-8} A/cm^2 at 0.8 MV/cm, likely due to the change of the film microstructure. Compared with 350°C annealing, higher-temperature annealing can improve the mechanical strength of the ultralow-k film, i.e., $E_r \approx 5$ GPa and $H \approx 0.56$ GPa after 500°C annealing.

Key words: Porous SiCOH film, ultralow dielectric constant, spin-coating, thermal annealing

INTRODUCTION

As the feature size decreases in ultralarge-scale integrated circuits, the parasitic resistance and capacitance coupling (RC delay) become the determining factors for signal propagation. To decrease the RC delay, low-dielectric-constant (low-k) materials have been used to replace conventional SiO_2 dielectric ($k \approx 4$) in advanced interconnect technology. According to the international technology roadmap for semiconductors (ITRS), 45 nm/32 nm technologies demand ultralow-k dielectrics with $2.0 < k < 2.7$.[1] On the other hand, to achieve global and local wafer planarity, the chemical-mechanical planarization (CMP) process is extensively used in the semiconductor industry. Therefore, the mechanical properties of the interlevel dielectrics (ILD), such as hardness and Young's modulus, are of critical importance for achieving a reliable CMP process. As one of the most promising ILD candidates, SiOCH dielectric films have been investigated extensively, and exhibit typical hardness of 0.13 GPa to 1.7 GPa and elastic moduli of 2.5 GPa to 12.2 GPa.[2–7]

It is well known that decreasing the polarizability and density of a bulk material can significantly reduce its dielectric constant; e.g., low-polarizability C–H, C–C, C–N, C–F bonds or pores/spaces are introduced into ultralow-k films. Among the various ultralow-k materials, porous SiCOH dielectric with many weak polar Si–C, C–C, and C–H bonds is

(Received March 24, 2011; accepted July 15, 2011; published online August 10, 2011)

considered one of the strong candidates for the 45 nm/32 nm technology nodes, including porous methyl silsesquioxane (MSQ), porous hydrogen silsesquioxane (HSQ), and porous carbon-doped oxide (CDO) films.[8–10] In general, incorporation of Si and C into low-*k* film is realized by adopting precursors containing Si and C atoms, while the formation of pore structure can be obtained by means of such methods as decomposition of sacrificial materials, phase separation, etching treatments, and utilization of ring-type precursors.[8,10–13] In recent years, chemical-vapor-deposited SiCOH films have been studied intensively as low-*k* dielectrics, exhibiting *k* values of 2.4 to 3.[12,13] However, it is still a challenge to achieve ultralow-*k* films with $k < 2.4$. On the other hand, many deposition techniques have been reported for the preparation of porous SiCOH films, of which spin-on deposition (SOD) is a method with great potential due to its excellent gap filling, good planarization, and low cost of ownership.[11]

In this work, to achieve lower *k* value, we introduced not only weak polar alkyl groups but also nanopores to reduce the polarizability of the matrix material and the film density. However, incorporation of nanopores would reduce the mechanical strength of porous films. To address the trade-off between dielectric constant and mechanical strength, the microstructures of low-*k* precursors should be engineered. Therefore, the bridged organosilicate precursor 1,2-bis(triethoxysilyl)ethane (BTEE) was employed to enhance the film toughness, as reported by Cham et al.[14] Accordingly, porous ultralow-*k* films with adequate mechanical strength were achieved. Further, the chemical structure and physical properties were investigated as a function of treatment temperature.

EXPERIMENTAL PROCEDURES

Preparation of Thin Films

Nanoporous SiCOH films were formed by spin-coating. The details of the preparation procedure are as follows: Firstly, the coating solution was prepared, being composed of 1,2-bis(triethoxysilyl)ethane (BTEE), triethoxymethylsilane (MTES), poly(ethylene oxide)–poly(propylene oxide)–poly(ethylene oxide) template (P_{123}), deionized water, ethanol (EtOH), and hydrochloric acid (HCl). For a typical solution, 1.037 g BTEE and 0.356 g MTES were mixed at 60°C, then a mixture of 0.556 g P_{123}, 2.813 g HCl (0.05 M), and 4.987 g EtOH was added to the above solution under stirring to obtain a sol solution. In this work, BTEE (96%), MTES (99%), and P_{123} were bought from Aldrich; EtOH and HCl were analytically pure. After stirring for a few hours, the resulting sol solution was cooled down to room temperature. Subsequently, the sol solution was spin-coated onto a cleaned low-resistance silicon (100) wafer with a resistivity of 0.001 Ω cm. After that, the spin-coated films were aged at 60°C for 70 h, followed by thermal treatment at 350°C for 2 h to remove the introduced template. Further, the thermal stability of the resulting film was investigated in the case of 400°C, 450°C, and 500°C annealing for 30 min, respectively, in a N_2 ambient. To extract the *k* value of the resulting film, metal–insulator–semiconductor (MIS) capacitors were fabricated, and circular Al electrodes with 800 μm diameter were formed by a shadow mask using an e-beam evaporator.

Characterization of Thin Films

X-ray diffraction (XRD) patterns of the films were recorded by using a small-angle x-ray scattering system (D/max-γB) operating with Cu K_α radiation (λ = 1.54 Å). Fourier-transform infrared (FTIR) spectrum measurements were carried out on the spectrometer (Thermo Fisher, Nicolet6700) in the mid-infrared region (4000 cm^{-1} to 400 cm^{-1}). Cross-section scanning electron microscopy (SEM; JEOL, JSM-6701F) was used to observe the matrix of the film. The film thickness was measured by a step profiler and confirmed by cross-sectional SEM. The surface morphology of the film was observed by atomic force microscopy (AFM; Veeco, Multimode-V).

The *k* value of the film was calculated according to the equation $k = Cd/\varepsilon_0 A$, where C is the capacitance of the MIS capacitor at 100 kHz, d is the thickness of the film, A is the area of the top electrode, and ε_0 is the permittivity of vacuum. Capacitance–voltage (C–V) and current–voltage (I–V) characteristics were measured using a Keithley 4200 instrument. The mechanical properties of the films were determined by means of an *in situ* nanomechanical test system (TI-700 Ubi; Hysitron, Inc.). The dynamic continuous function was adopted to measure load–displacement curves. With a Berkovich tip, the indentation displacement was less than 1/10 of the thickness of the measured films.

RESULTS AND DISCUSSION

Characterization of Film Morphology

In general, to achieve ultralow *k* less than 2.6, Si–O-dominant dielectrics must be porous. Figure 1 shows a cross-section SEM image of the resulting film. It is seen that the resulting film exhibits a fluey cross-section, i.e., a nanoporous matrix. Figure 2 shows XRD patterns of films annealed at different temperatures in comparison with an as-coated film. It is found that only a weak diffraction peak appears at 2θ = 0.90° for the unannealed film. After 350°C thermal treatment, a strong and sharp diffraction peak at 2θ = 1.60° is observed together with a small peak at 2θ = 3.20°. This indicates that a highly ordered two-dimensional (2D) hexagonal pore structure is formed.[15] Much research has also indicated that the resulting periodic mesoporous structure usually exhibits a 2D hexagonal shape when using

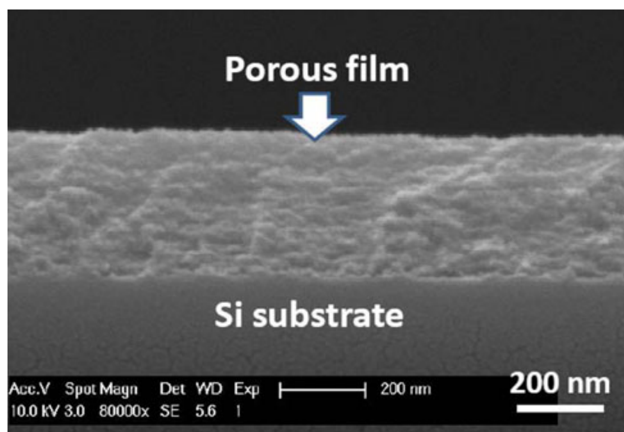

Fig. 1. Cross-section SEM image of the resulting film.

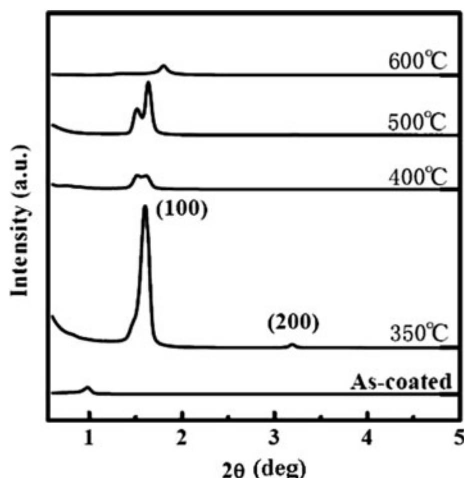

Fig. 2. XRD patterns of as-coated film and films annealed at different temperatures.

organosilica precursors and the supramolecular template P_{123} under acidic conditions.[16] Further, based on the strong diffraction peak of the (100) plane, the unit cell parameter was calculated as a = 6.4 nm according to Eq. (1).[10]

$$a = 2d\Big/\sqrt{3};\, d = 55.1\text{A}. \quad (1)$$

As the annealing temperature was increased to 400°C, the strong diffraction peak became two adjacent small peaks at 2θ = 1.50° and 1.60°. Further, the two weak peaks evolved into one small peak at 2θ = 1.51° and one strong peak at 2θ = 1.64° in the case of 500°C annealing. It is difficult to attribute the splitting of the strong peak to some given structure, but it can be concluded that the characteristics of the foregoing pores are changed after 400°C to 500°C annealing, which is likely due to shrinkage and deformation of the pores incurred by high-temperature annealing. When the annealing temperature was increased to 600°C, the original diffraction peak nearly disappeared, reflecting that the initial hexagonal pores were almost destroyed.

The surface morphologies of the films treated at different temperatures are shown in Fig. 3. It is seen that all the annealed films exhibit a crack-free surface, even after 500°C annealing. Moreover, all the films have a smooth surface, as demonstrated by the root-mean-square (RMS) roughness below 0.17 nm. In particular, after annealing at 400°C and 500°C, the resulting films display improved RMS roughness, i.e., as low as 0.117 nm and 0.113 nm, respectively. This should be related to surface rearrangement of the organic groups incurred by heating, such as cross-linking between chemical bonds and shrinkage of the pores.

FTIR Analyses of the Films

To study the effect of annealing temperature on the chemical composition of the nanoporous films, FTIR spectra were recorded for as-coated and annealed films, as shown in Fig. 4. For the as-coated film, one absorption band was observed in the range of 3000 cm^{-1} to 2800 cm^{-1}, which is attributed to C–H stretching vibration mainly originating from the introduced template molecules. The strongest absorption peak between 1200 cm^{-1} and 1000 cm^{-1} is associated with the Si–O–Si configuration, which contributes a lot to the framework of the nanoporous film. The absorption peak at 1270 cm^{-1} results from $-CH_3$ symmetrical deformation vibration in $Si–CH_3$, and the peaks centered at 780 cm^{-1} and 760 cm^{-1} correspond to the C–H rocking vibration in $Si–CH_3$ and $CH_2–CH_2$, respectively.[13,17,18] The broad absorption band near 3400 cm^{-1} correlates with the hydroxyl vibration, and the peak at 920 cm^{-1} is ascribed to the Si–OH groups.[10,13] After annealing at 350°C for 2 h, the absorption peak between 3000 cm^{-1} and 2800 cm^{-1} almost disappears. This indicates that the thermal treatment at 350°C can effectively remove the template molecules embedded in the film. Meanwhile, the absorption peak associated with Si–OH groups cannot be observed, which could be attributed to condensation reaction between hydrophilic Si–OH groups, thus leading to the formation of cross-linking Si–O–Si network structure as well as volatilization of the byproduct H_2O. Therefore, it is anticipated that both the resistance to water absorption and mechanical strength of the films are improved after the aforementioned thermal treatment. Moreover, the strong absorption peak in the range of 1200 cm^{-1} to 1000 cm^{-1} exhibits an obvious change compared with the as-coated film; i.e., the weak peak at 1030 cm^{-1} for the as-coated film becomes one enhanced peak at 1050 cm^{-1} for the film annealed at 350°C, while the intense peak at 1100 cm^{-1} becomes a shoulder. This should be attributed to the formation of more Si–O–Si bonds

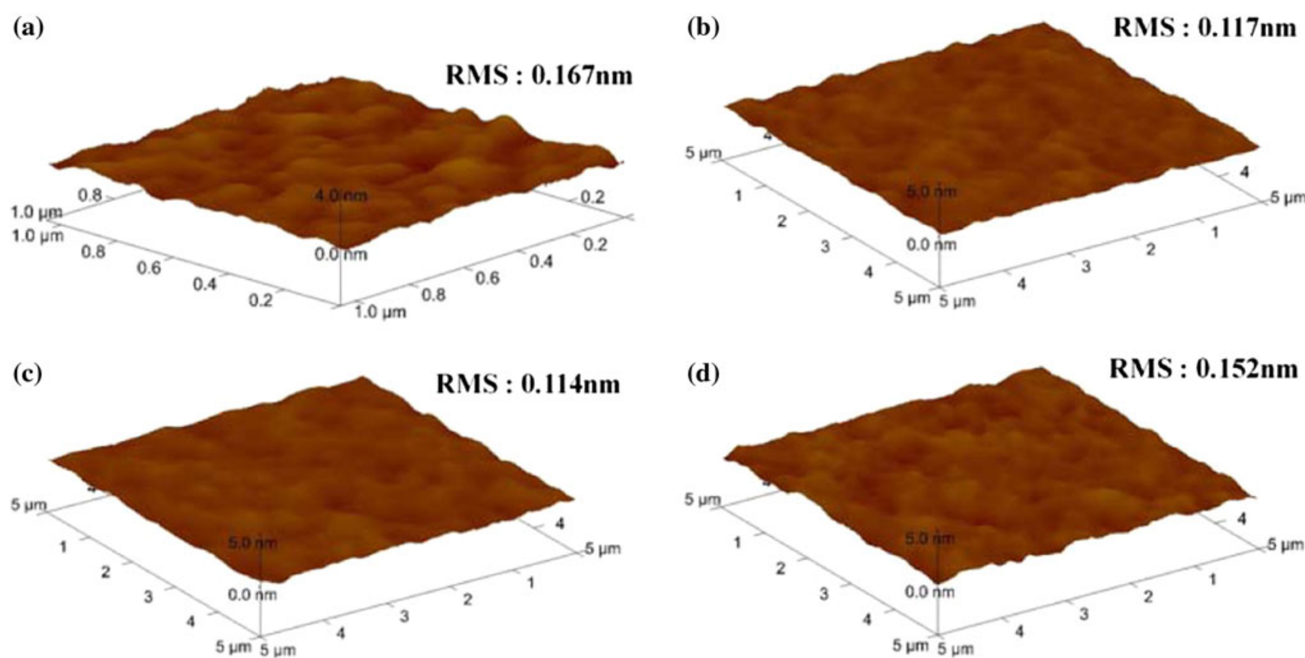

Fig. 3. AFM surface images of the resulting films corresponding to (a) 350°C, (b) 400°C, (c) 450°C, and (d) 500°C, respectively.

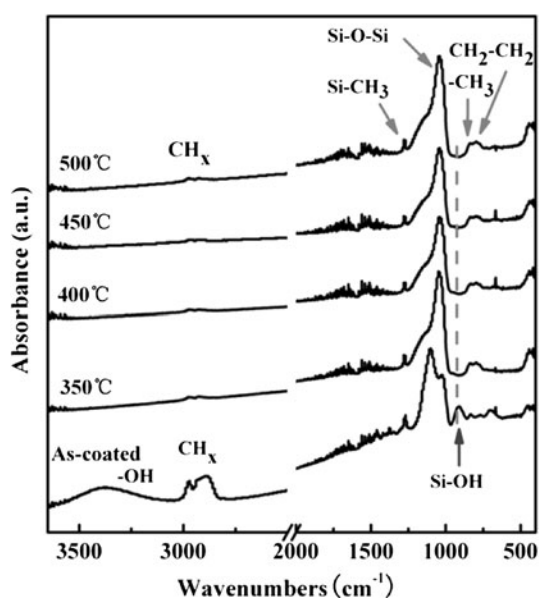

Fig. 4. FTIR patterns of as-coated and annealed films at different temperatures.

as well as the removal of the template molecules, which contain C–H and C–O–C bonds, corresponding to the absorption peaks in the range of 3000 cm^{-1} to 2800 cm^{-1} and 1200 cm^{-1} to 1000 cm^{-1},[19] respectively. The presence of the peaks at around 1270 cm^{-1}, 780 cm^{-1}, and 760 cm^{-1} indicates that the organic CH_x groups are incorporated into the film framework. As the annealing temperature was increased up to 500°C, the resulting FTIR spectra hardly exhibit any observable differences from each other, hence revealing that the resulting nanoporous SiCOH film has good thermal stability. This is also confirmed by the relatively stable ratio of (Si–CH_3 + CH_x)/Si–O for different annealing temperatures (i.e., 3.0% to 3.4%), as deduced from the corresponding peak areas in FTIR, as shown in Table I.

In general, the absorption peak in the range of 1300 cm^{-1} to 950 cm^{-1} is usually used to define the relative concentrations of various Si–O bonding configurations such as Si–O–Si cage and network etc.[20–22] Therefore, in the present work, the wide

Table I. Peak area ratio of (Si–CH_3 + CH_x)/Si–O for films annealed at different temperatures

Annealing Temperature (°C)	350	400	450	500
Peak area of Si–CH_3 (1300 cm^{-1} to 1275 cm^{-1})	0.182	0.153	0.145	0.182
Peak area of CH_x (3000 cm^{-1} to 2800 cm^{-1})	0.263	0.214	0.183	0.249
Peak area of Si–O (1255 cm^{-1} to 960 cm^{-1})	13.943	10.695	10.866	14.075
Peak area ratio of (Si–CH_3 + CH_x)/(Si–O)	3.2%	3.4%	3.0%	3.1%

absorption peak between 1250 cm^{-1} and 960 cm^{-1} was deconvoluted into three Gaussian components in the case of different annealing temperatures, as shown in Fig. 5. They are centered at 1019 ± 1 cm^{-1}, 1046 ± 1 cm^{-1}, and 1119 ± 1 cm^{-1}, and attributed to the Si–O stretching vibration in C–Si–O open link (bond angle <144°), Si–O–Si network (bond angle ~144°), and cage (bond angle ~150°), respectively.[20,21] According to the areas of the fitted subpeaks, the relative concentrations of all the components were calculated, as presented in Fig. 5. It is found that the relative contents of both cage and network Si–O–Si configurations are much larger than that of the open link C–Si–O configuration for the films annealed at different temperatures, i.e., 43% to 47% versus 10% to 12%. Moreover, the relative concentrations of Si–O–Si cage and network configurations exhibit a slight fluctuation with annealing temperature, indicating good stability of the chemical bonds against annealing. The three aforementioned types of Si–O structures are presented schematically in Fig. 6. In a word, high content (~43%) of the cage Si–O–Si structure is achieved in the resulting film, which can reduce the dielectric constant of the film to a large extent due to the free volume created. Meanwhile, the presence of sufficient Si–O–Si network structure is also beneficial to improve the mechanical strength of the nanoporous film.

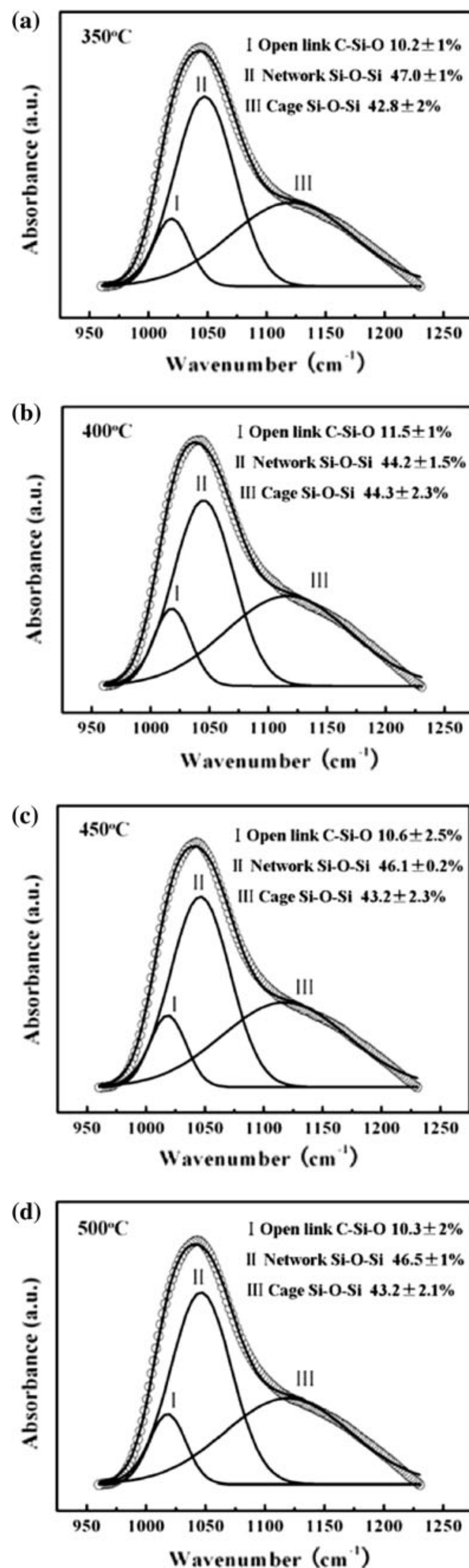

Fig. 5. Deconvolution of the Si–O stretching band (1230 cm^{-1} to 960 cm^{-1}) illustrated in Fig. 4 for SiCOH films annealed at different temperatures.

Electrical and Mechanical Characteristics of the Films

The dielectric constants (k values) of the resulting nanoporous films are shown in Fig. 7 as a function of annealing temperature. For 2-h thermal treatment at 350°C, the resulting film exhibits an ultralow k value of ~2.0. Further, as the annealing temperature was increased from 400°C to 500°C, the resulting k value remained in the ultralow k range of 1.85 to 2.22. Such an ultralow k value should be attributed to the incorporation of nanopores and low-polarizability chemical bonds into the film matrix. In terms of the incorporated nanopores, two factors contribute to the formation of nanovoids. One is the thermal decomposition of the template molecules, and the other is the formation of the cage frameworks due to chemical reactions between the precursors, as shown in Fig. 6b. Moreover, the presence of Si–C, C–C, and C–H bonds also plays an important role in reducing the k value as a result of lower polarizability.

Figure 8 shows the dependence of leakage current density on electric field for a low-k film annealed at 350°C for 2 h. It is found that the leakage current density at 1 MV/cm is as low as 3×10^{-8} A/cm^2. When the annealing temperature was increased to 400°C, the resulting leakage current density exhibits a rise of one order of magnitude. However, after 500°C annealing, the resulting leakage current returns to a lower level; for instance, it is equal

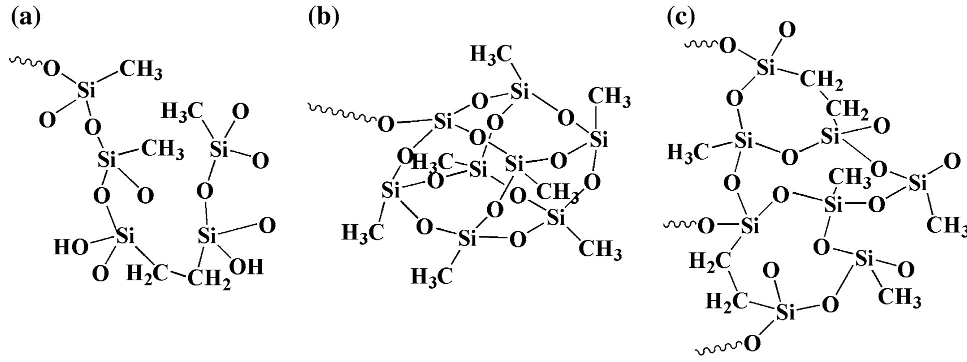

Fig. 6. Schematic diagrams of the backbone structure of the SiCOH film. A, B, and C represent open-link C–Si–O, cage Si–O–Si, and network Si–O–Si configurations, respectively.

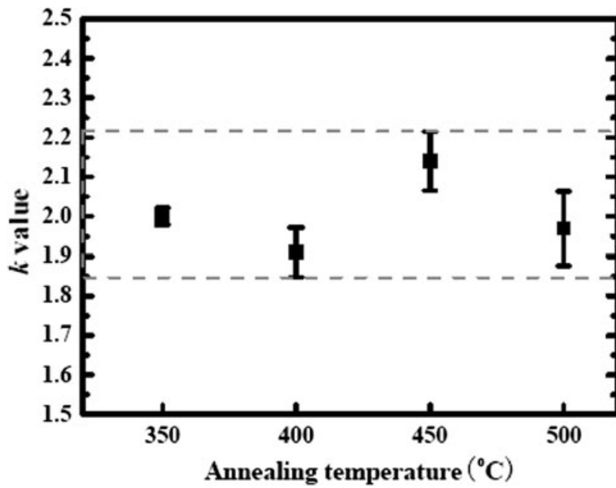

Fig. 7. Extracted *k* values of the resulting porous SiCOH films as a function of annealing temperature.

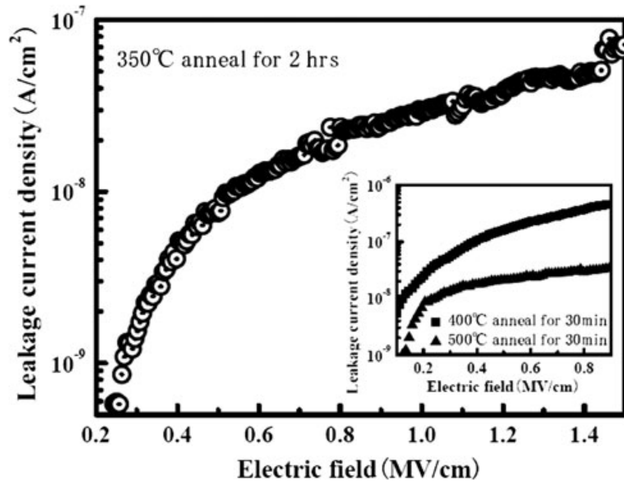

Fig. 8. Dependence of leakage current density on electric field for film annealed at 350°C for 2 h. The inset shows the leakage characteristics of the films annealed at 400°C and 500°C for 30 min, respectively.

to 3×10^{-8} A/cm^2 at 0.8 MV/cm. The above phenomena are likely due to the change of the film microstructure, as revealed in Figs. 2 and 5.

The reduced modulus (E_r) and hardness (H) of the low-k films were calculated according to Eqs. (2–4).

$$E_r = \frac{\sqrt{\pi}}{2\sqrt{A(h_c)}}S, \tag{2}$$

$$H = \frac{P_{max}}{A(h_c)}, \tag{3}$$

$$h_c = h_{max} - 0.75\frac{p_{max}}{S}, \tag{4}$$

where $A(h_c)$ is the contact area at contact depth h_c, calibrated using a reference sample of fused silica. P_{max} and h_{max} represent the maximum load and indentation displacement. S is the contact stiffness extracted from the slope of the initial unloading portion.

Figure 9 illustrates the cumulative distributions of the extracted E_r and H values for different annealing temperatures. It is seen that the low-k film annealed at 350°C has a reduced modulus of 4.05 GPa for 60% probability, as shown in Fig. 9a. Further, elevating the annealing temperature can enhance the E_r value of the film; for example, E_r was 6.21 GPa and 5.00 GPa after 400°C and 500°C annealing, respectively, for 60% probability. Figure 9b reflects the evolution of the hardness with annealing temperature. For 350°C annealing, the resulting film hardness was 0.32 GPa for 60% probability. Further, as the annealing temperature was increased, H exhibited a gradual rise, reaching 0.52 GPa and 0.56 GPa, respectively, for 400°C and 500°C annealing for 60% probability. In a word, both E_r and H of the ultralow-k films improve after being annealed at temperatures higher than 350°C, which is mainly due to the microstructure change and inner rearrangement of the films incurred by annealing treatment. Moreover, the phenomenon that annealing at 400°C can lead to a larger E_r than that at 500°C can be explained as follows: The mechanical properties of the films can be reasonably interpreted within the framework of the continuous

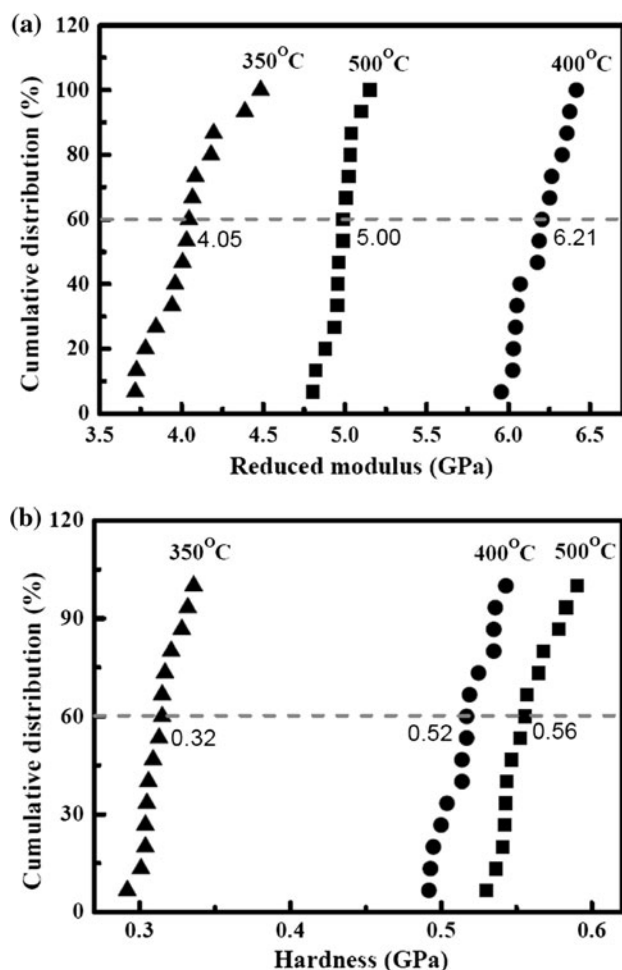

Fig. 9. Cumulative distribution of (a) reduced modulus and (b) hardness of low-*k* films annealed at different temperatures.

random network theory and percolation of rigidity concepts.[23,24] The percolation of rigidity defines a compositional point in a network where the system transitions from a nonrigid state to a rigid one, and the aforementioned compositional point is related to the atomic bonding configurations such as open link, network, and cage structures. In our case, the films annealed at 500°C could be more rigid and less able to "spring back" after deformation due to the increased crosslinking and rigidity imparted during the annealing process.[2] This is also reflected by the change of the pore structure, as shown in Fig. 2. As we know, lower-*k* films are achieved generally at the expense of their mechanical strength, especially for ultralow-*k* films with $k < 2.3$. It is reported that porous MSQ films with $k = 2$ have a modulus (E) of ~3 GPa.[3,25] In our case, the ultralow *k* value of ~1.9 was achieved for a film annealed at 400°C, and the calculated E was approximately 5.9 GPa, thus indicating a promising candidate for future ILD.

CONCLUSIONS

Porous SiCOH films were prepared using BTEE, MTES, and a triblock copolymer template P_{123} by means of a spin-coating technique. It was found that the resulting film annealed at 350°C for 2 h in N_2 exhibits an ultralow k value of ~2.0, which is attributed to the incorporation of nanopores and low-polarizability chemical bonds into the film matrix. Moreover, a leakage current density of 3×10^{-8} A/cm^2 at 1 MV/cm is achieved, as well as $E_r \approx 4.05$ GPa and $H \approx 0.32$ GPa. After being annealed between 400°C and 500°C for 30 min, the resulting films still showed ultralow k values of 1.85 to 2.22 and leakage current densities of 3.7×10^{-7} A/cm^2 to 3×10^{-8} A/cm^2 at 0.8 MV/cm. These fluctuations in the k value and leakage current likely correlate with the changes of the film microstructure such as the shape and arrangement of the pores and the relative content of the cage Si–O–Si structure. Further, compared with 350°C annealing, higher-temperature annealing can improve the mechanical strength of the ultralow-k film, i.e., $E_r \approx 5$ GPa and $H \approx 0.56$ GPa for 500°C annealing.

ACKNOWLEDGEMENT

The authors acknowledge the financial support from the National Key Technologies R&D Program of China (Grant No. 2011ZX02703-04).

REFERENCES

1. M. Tata, Y. Harada, and T. Tamura, *IEDM Tech. Dig.* 845 (2003).
2. D.D. Burkey and K.K. Gleason, *J. Appl. Phys.* 93, 5147 (2003).
3. S. Yang, P.A. Mirau, C.S. Pai, and O. Nalamasu, *Chem. Mater.* 14, 372 (2002).
4. N. Tajima, T. Ohno, T. Hamada, K. Yoneda, N. Kobayashi, S. Hasaka, and M. Inoue, *Appl. Phys. Lett.* 89, 061907 (2006).
5. A. Grill and V. Patel, *Appl. Phys. Lett.* 79, 803 (2001).
6. A. Grill, *J. Appl. Phys.* 93, 1785 (2003).
7. J. Lubguban, T. Rajagopalan, N. Mehta, B. Lahlouh, S.L. Simon, and S. Gagopadhyay, *J. Appl. Phys.* 92, 1033 (2002).
8. L.L. Chapelon, V. Arnal, and M. Broekaart, *Microelectron. Eng.* 76, 1 (2004).
9. V. Jousseaume, L. Favennec, A. Zenasni, and O. Gourhant, *Surf. Coat. Technol.* 201, 9249 (2007).
10. A. Majumdar, G. Das, and N. Patel, *J. Electrochem. Soc.* 155, D22 (2008).
11. K. Maex, M.R. Baklanov, and D. Shamiryan, *J. Appl. Phys.* 93, 8800 (2003).
12. B.D. Hatton, K. Landsdron, and W.J. Hunks, *Mater. Today* 9, 24 (2006).
13. T.B. Casserly and K.K. Gleason, *Plasma Process. Polym.* 2, 680 (2005).
14. B.J. Cham, B. Kim, and B. Jung, *J. Non Cryst. Solids* 352, 5681 (2006).
15. B. Toury and F. Babonneau, *J. Eur. Ceram. Soc.* 25, 265 (2005).
16. F. Hoffmann, M. Cornelius, J. Morell, and M. Fröba, *Angew. Chem. Int. Ed.* 45, 3216 (2006).
17. W.Y. Leong, C.F. Tsang, and H.Y. Li, *Thin Solid Films* 496, 403 (2006).
18. H.W. Su and W.C. Chen, *Mater. Chem. Phys.* 114, 738 (2009).
19. B. Bharatiya, C. Guo, and J.H. Ma, *Eur. Polym. J.* 43, 1886 (2007).
20. T.K.S. Wong, B. Liu, and B. Narayanan, *Thin Solid Films* 462–463, 158 (2004).

21. Y. Shioya, T. Ohdaira, and R. Suzuki, *J. Non Cryst. Solids* 354, 2978 (2008).
22. C.S. Yang, Y.H. Yu, and K.M. Lee, *Thin Solid Films* 506–507, 52 (2006).
23. J.C. Phillips, *J. Non Cryst. Solids* 34, 153 (1979).
24. M.F. Thorpe, *J. Non Cryst. Solids* 57, 355 (1983).
25. A.R. Balkenende, F.K. de Theije, and J.C.K. Kriege, *Adv. Mater.* 15, 139 (2003).